

## Article

# On the Effect of Volumetric Energy Density on the Characteristics of 3D-Printed Metals and Alloys

Eleftheria Maria Pechlivani <sup>1,\*</sup>, Lazaros Melidis <sup>2</sup>, Sotirios Pemas <sup>1</sup>, Konstantinos Katakalos <sup>2</sup>,  
Dimitrios Tzovaras <sup>1</sup> and Avraam A. Konstantinidis <sup>3</sup>

<sup>1</sup> Centre for Research and Technology Hellas, Information Technologies Institute, 6th km Charilaou-Thermi Road, 57001 Thessaloniki, Greece; sopemas@iti.gr (S.P.); dimitrios.tzovaras@iti.gr (D.T.)

<sup>2</sup> Laboratory of Experimental Strength of Materials and Structures, School of Civil Engineering, Faculty of Engineering, Aristotle University of Thessaloniki, 54124 Thessaloniki, Greece; lazmelidis@gmail.com (L.M.); kkatakal@civil.auth.gr (K.K.)

<sup>3</sup> Laboratory of Engineering Mechanics, School of Civil Engineering, Faculty of Engineering, Aristotle University of Thessaloniki, 54124 Thessaloniki, Greece; akonsta@civil.auth.gr

\* Correspondence: riapechl@iti.gr; Tel.: +30-2311-257751

**Abstract:** Selective Laser Melting (SLM) is a specific 3D printing technique under Additive Manufacturing (AM) metal technologies. SLM is considered to be a precise rapid AM process combined with a powder bed system for producing customized metal products with a tailored microstructure and shape. Differences in the printing parameters can lead to differences in the surface as well as macroscopic mechanical characteristics of the manufactured parts and components. This work aims at quantifying the effect of the Volumetric Energy Density (VED) used in the SLM processing of various metals and alloys. Metallic specimens printed with different VED values were subjected to surface characterization as well as tensile deformation. Their surface roughness, yield stress and toughness were subsequently used to verify a linear relationship between roughness and VED, and a linear behavior between yield stress/toughness and VED was proposed. Predictive models were formulated for estimating the roughness/yield stress/toughness of the produced specimens with respect to the VED used in their production. The models' predictions will provide insight into the 3D printing parameters, thus minimizing the cost and effort of the 3D printing procedure, in applications where surface quality and strength are important.

**Keywords:** CoCrMo alloy 75A; stainless steel 316L-A; stainless steel 17-4PH-A; selective laser melting; SLM; 3D printing; tensile behavior; surface roughness



**Citation:** Pechlivani, E.M.; Melidis, L.; Pemas, S.; Katakalos, K.; Tzovaras, D.; Konstantinidis, A.A. On the Effect of Volumetric Energy Density on the Characteristics of 3D-Printed Metals and Alloys. *Metals* **2023**, *13*, 1776. <https://doi.org/10.3390/met13101776>

Academic Editor: Matteo Benedetti

Received: 25 August 2023

Revised: 1 October 2023

Accepted: 17 October 2023

Published: 20 October 2023



**Copyright:** © 2023 by the authors. Licensee MDPI, Basel, Switzerland. This article is an open access article distributed under the terms and conditions of the Creative Commons Attribution (CC BY) license (<https://creativecommons.org/licenses/by/4.0/>).

## 1. Introduction

Over the past decade, the Selective Laser Melting (SLM) technique, which belongs to the Additive Manufacturing (AM) metal technologies [1], has emerged as one of the most robust AM techniques for producing metal parts. It stands out as a prevalent technique under the umbrella of Powder Bed Fusion (PDF) processes, according to ISO/ASTM 52900–15 standards [1], leading to extensive exploration across various industries for the manufacturing of complex geometries and advanced design features [2–5]. SLM offers the versatility of processing a wide range of materials [6], including Al, Ti, Ni, Co, Cu, and Fe [7,8]. This technique involves a sequential layer-by-layer process, where the feedstock material in powder form is spread on the build platform, and the laser beam selectively melts the powder particles in each layer. This process continues until all layers are melted to form the final 3D-printed part [9–11]. The versatility it provides has resulted in its widespread adoption in diverse industries, including aerospace [12] and automotive [13], enabling the production of lightweight and intricate parts with minimized material waste [14]. Moreover, the medical field extensively utilizes SLM techniques for

creating patient-specific implants and medical devices, offering customized solutions to enhance patient outcomes [15–17].

To make efficient use of the SLM technique, it is necessary to have a thorough understanding of the optimal printing process parameters for each material in order to achieve optimized results [18]. The mechanical behavior of the final 3D-printed part is determined by the 3D printing process and the selected parameters [19,20]. Mechanical behavior can be assessed through various mechanical tests, such as the tension test [19,21]. Among the set of parameters, the Volumetric Energy Density (VED) value is particularly crucial and has a significant impact on mechanical performance [19,22,23]. VED is calculated based on the laser power ( $W$ ), scan speed ( $mm/s$ ), hatching distance ( $\mu m$ ), and layer thickness ( $\mu m$ ) [3,19]. Conducting extensive research is essential to determine the optimal values for each parameter depending on the print material.

Ghayoor et al. [24] investigated the impact of VED on the microstructure, texture, and mechanical properties of 304L stainless steel. The results revealed significant differences in the mechanical properties with varying VED values. Furthermore, a comprehensive review conducted by Kladovasilakis et al. [9] examined the influence of printing parameters on the quality of the final metal product. The study emphasized the importance of mechanical behavior, dimensional accuracy, and surface quality in determining part quality. Surface quality and dimensional accuracy were found to be greatly affected by build orientation and component geometry [25]. Moreover, the properties of the powder used in the process played a crucial role in determining the surface roughness, dimensional accuracy, and mechanical properties of 3D-printed metal parts. Moreover, Fotovatti et al. [4] emphasized the relationship between high surface quality and low layer thickness. Pechlivani et al. [19] examined the mechanical response of 3D-printed Inconel 718 to varying VED values, observing that mechanical behavior and surface roughness were dependent on VED. The authors highlighted that optimizing 3D-printed parts depends on the relationship between VED and mechanical response, as well as surface roughness. Furthermore, the final 3D-printed part's quality is influenced by two phenomena: lack of fusion and the keyhole effect, which are directly related to VED parameters. Lack of fusion occurs when VED is insufficient to fully melt the feedstock material and the material already built close to the surface, preventing uniform melting. On the other hand, the keyhole effect arises when VED is too high, leading to regions with entrapped gases within the 3D-printed part's geometry [3,24,26].

In this study, the objective is to contribute to a broader understanding of the impact of VED values in the SLM technique. To achieve this, three metallic materials were examined as feedstock materials in an SLM 3D Printer: stainless steel 316L-A, stainless steel 17-4PH-A, and cobalt–chromium–molybdenum alloy. Various parameters were adjusted to ensure a suitable range of VED values for each material. Through thorough analysis, the aim is to establish the correlation between VED values, mechanical properties, and roughness in order to draw conclusions about the possibly linear relationship that exists among these factors. The novelty of this work lies in the presentation of results for three different metallic materials and the comparison of the level of the aforementioned linearity present in each material.

This paper is structured as follows: Section 2 provides the materials and methods used in the study. Section 3 includes the results of mechanical testing and surface roughness measurements. Also, the correlation between VED and roughness/mechanical properties is presented and discussed. Finally, the study concludes in Section 4. A diagram of the present study is given in Figure 1.

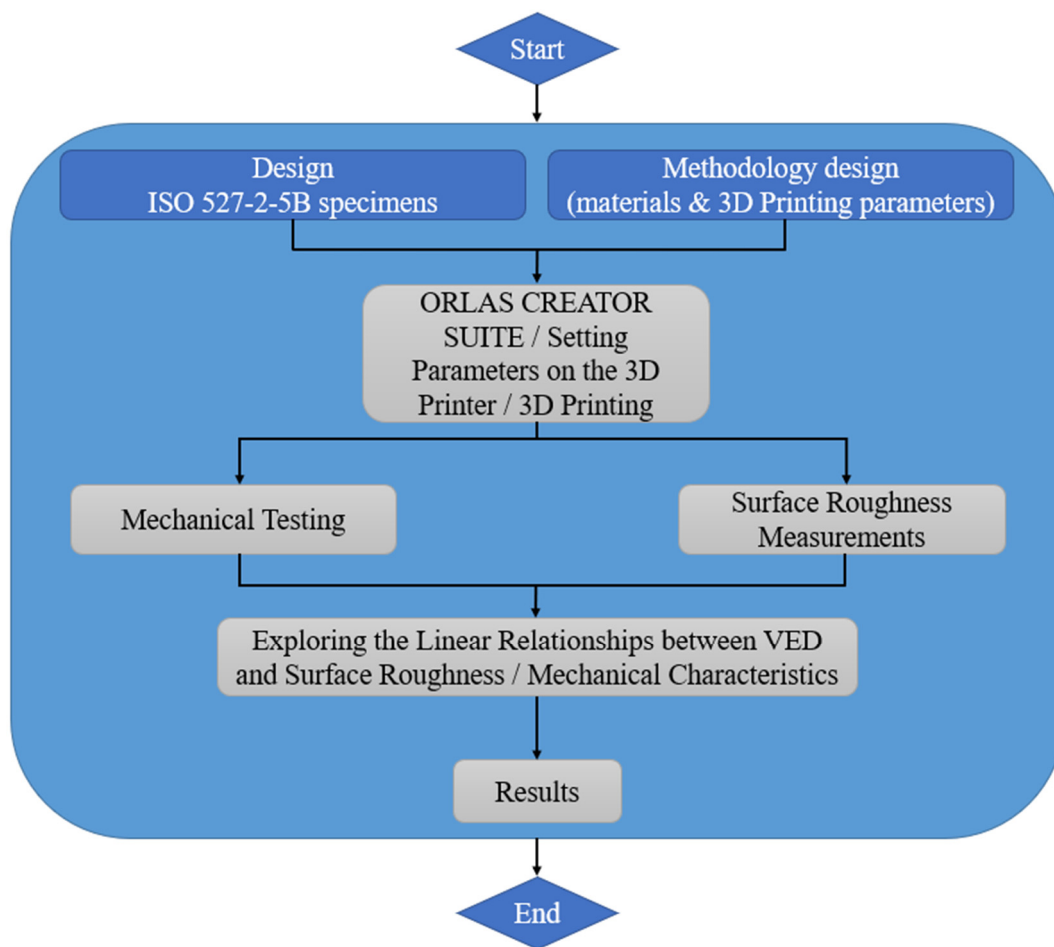


Figure 1. Architectural diagram of the present study.

## 2. Methodology

### 2.1. Additive Manufacturing

The ORLAS CREATOR 3D printer (OR Laser, Germany) was employed for manufacturing the printed specimens using the SLM technique. The feedstock for the specimens' manufacture consisted of metallic powder supplied by the Oerlikon company, including MetcoAdd 75A (a cobalt–chromium–molybdenum-based powder similar to ASTM F75, ISO 5832-4, and UNS R31538, Nominal Chemistry: Co 28Cr 6Mo) [27], MetcoAdd 316L-A (an austenitic steel powder with chemistry similar to EN 1.4404 and UNS S316603, Nominal Chemistry: Fe 18Cr 12Ni 2Mo 0.02C) [28], and MetcoAdd 17-4PH-A (a martensitic, precipitation-hardening stainless steel powder with chemistry similar to AMS 5643, Nominal Chemistry: Fe 17Cr 4.5Ni 4Cu 0.3(Nb/Ta) 0.07C) [29]. These powders were examined for the manufacturing of specimens and were tested for their mechanical properties.

The tested dog-bone-shaped specimens ISO 527-2-5B were designed using SOLIDWORKS® CAD Software (2022 SP2.0 Professional version) with dimensions of  $35 \times 6 \times 1 \text{ mm}^3$ . To optimize the mechanical properties in the XY direction [24,30], the specimens were printed vertically. The arrangement of the specimens on the ORLAS CREATOR build platform was performed through ORLAS SUITE software (Version 6.1.0.13 rc13579), which was also used to set the 3D printing parameters. The gap between the specimens and the build platform, serving as a support for required adhesion, was set at 3 mm, while the distance between the specimens was set at 5 mm.

The VED calculation was determined using the VED formula

$$VED = \frac{P}{v \times h \times t} \times 10^6 \text{ J/mm}^3 \quad (1)$$

where  $P$  represents the laser power (W),  $v$  denotes the scan speed (mm/s),  $h$  signifies the hatching distance ( $\mu\text{m}$ ), and  $t$  indicates the layer thickness ( $\mu\text{m}$ ). The hatching distance, layer thickness, and spot size parameters were kept constant throughout all experiments. The variation in VED values in this study was achieved solely by adjusting the laser power and scan speed parameters. An increase in the value of VED could be achieved by decreasing the scan speed  $v$  or by increasing the laser power  $P$ .

Table 1 presents a summary of all the parameters used to manufacture the different specimens, resulting in a wide range of VED values. For each material, three 3D prints were conducted, resulting in 4 specimens in each print, with a combination of the laser power and scan speed values (Table 1). In general, an increase in the VED value, as calculated by Equation (1), can be achieved by either reducing the scan speed ( $v$ ) or increasing the laser power ( $P$ ). In our study, we maintained constant values for hatching distance and layer thickness parameters. From Table 1, it can be concluded that a lower scan speed (higher VED value), would be expected to lead to the production of better quality specimens (better mechanical performance). The same would be expected to be true also for the surface quality of the specimens, i.e., a lower scan speed should lead to the production of better surface quality specimens. However, this holds true up to a specific VED value. Beyond this limit, the surface quality deteriorates because all powder particles have melted, leading to surface irregularities and increased roughness. Table 1 further demonstrates that the highest VED value within the considered range is achieved with the lowest scan speed and the highest laser power. Especially, the findings of the present study are limited to a specific range of VED values from 80 to 190.476 J/mm<sup>3</sup>.

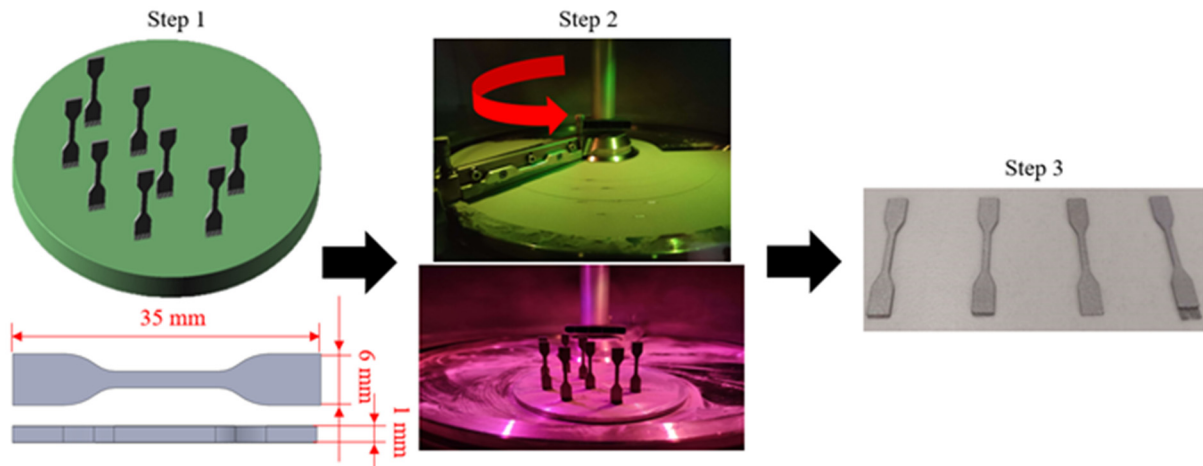
**Table 1.** 3D printing parameters for the 3D-printed specimens.

Material	Batch	Laser Power (W)	Scan Speed (mm/s)	VED (J/mm <sup>3</sup> )	Hatching Distance ( $\mu\text{m}$ )	Layer Thickness ( $\mu\text{m}$ )	Spot Size ( $\mu\text{m}$ )	Number of Specimens
CoCrMo	S1	105	630	166.666	40	25	40	4
	S2	120	850	141.176	40	25	40	4
	S3	120	630	190.476	40	25	40	4
SS316L-A	S1	125	1000	125	40	25	40	4
	S2	140	1300	107.692	40	25	40	4
	S3	140	1000	140	40	25	40	4
SS17-4PH-A	S1	110	1200	91.666	40	25	40	4
	S2	120	1500	80	40	25	40	4
	S3	120	1200	100	40	25	40	4

Within the 3D printer, a tank containing the feedstock material in powder form is present. This tank moves upwards with a step equal to the layer height, and the powder is evenly distributed using a rubber coater on the building platform. The laser beam then follows a predetermined path, melting the metallic powder particles and creating a solid layer of the final part. Once the melting process is complete, the building platform moves downwards to allow the new layer of powder to spread over it. This entire process is repeated for the number of layers required to construct the final part [19].

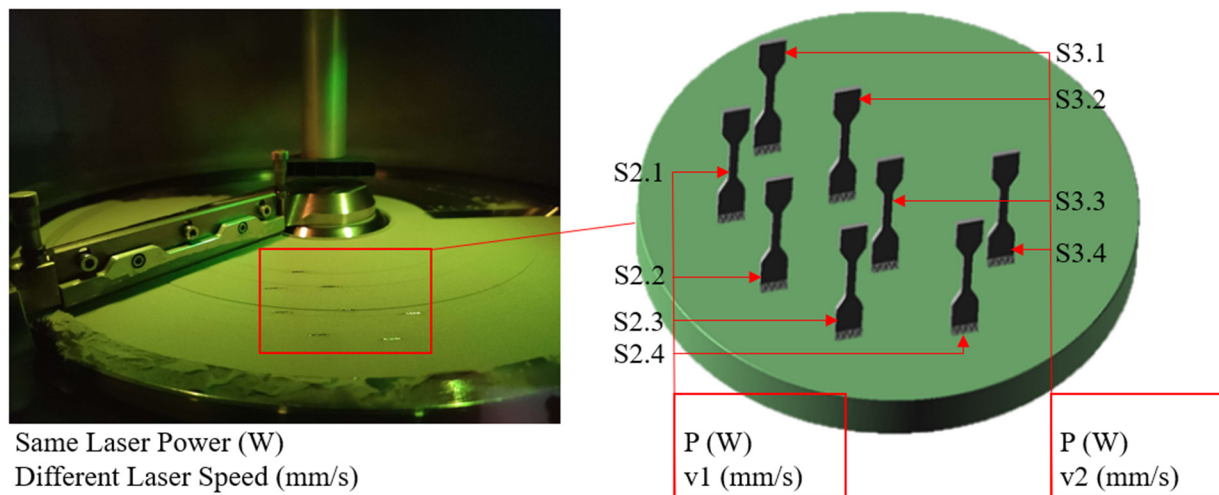
Within the print chamber, the specimens were positioned in the optimized location in accordance with the software to ensure the success of the 3D printing process. The distance between them was strategically considered to avoid failures caused when two parts are positioned too closely, avoiding the impact of heat generated during the printing of the neighboring part. The arrangement of the specimens played a crucial role in ensuring the desired quality and accuracy in the final 3D-printed parts.

Figure 2 illustrates the steps that constitute the entire process employed for manufacturing the specimens. In the initial phase, denoted as step 1, the specimens were designed and the parameters were configured within the slicer software. In step 2, the 3D printing process commenced within the ORLAS CREATOR chamber, wherein the rotational movement of the coater in each layer followed the direction indicated by the arrow. Finally, in step 3, the printed specimens were prepared to undergo mechanical and characterization tests.



**Figure 2.** Steps of 3D-printing the specimens using the SLM technique.

Figure 3 illustrates the location of the S2 and S3 specimens on the build platform during the SLM process. This figure depicts the arrangement of the specimens in each print, comprising a total of eight specimens, all having the same laser power but with two different scan speeds.



**Figure 3.** Distribution of tensile specimens on the build platform.

After detaching the specimens from the build platform, it is necessary to remove the supporting structures, which, in this particular case, are located on one side of the specimens, and to clean the specimens of any remaining powder. It was observed that specimens of the same material exhibited visual differences from each other, which is attributed to the different VED values. The varying speed and power of the laser during the melting process resulted in distinct outcomes that are distinguishable both visually and through mechanical property tests.

## 2.2. Surface Characterization

A series of confocal microscopy measurements were performed on the three different sets of 3D-printed metals, i.e., CoCrMo, SS316L-A, SS17-4PH-A. This was completed to assess the effect of the VED on surface roughness. The confocal measurements were executed using a Leica DSM8 confocal microscope (Leica Microsystems, Wetzlar, Germany). The measurements were taken at three different locations on the surface of each sample, as shown in the schematic of Figure 4, in order to have roughness data representative of the whole specimens' surface.

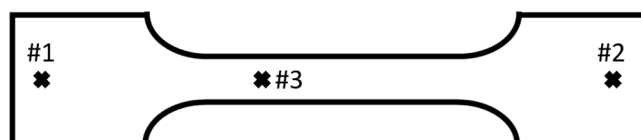


Figure 4. Specimen surface locations for confocal measurements.

Three magnifications were used, namely  $\times 5$ ,  $\times 10$ , and  $\times 20$ , and various roughness measures were calculated according to ISO25178 ( $S_q$ ,  $S_{sk}$ ,  $S_{ku}$ ,  $S_p$ ,  $S_v$ ,  $S_z$ ,  $S_a$ ), from which  $S_a$  was considered to be the most representative one.

## 2.3. Mechanical Characterization

A series of tensile tests was performed on the three kinds of 3D-printed metals at hand. Three different specimens of each metal were tested under uniaxial tensile loading.

The experimental procedure included positioning each specimen between the grips of the testing machine, Instron model 5969 (Instron, Norwood, MA, USA), and the application of the uniaxial tensile load through the employed electric jack by imposing a relatively slow uniaxial displacement rate (0.5 mm/min) [31]. During the experiment, the variation of the applied load ( $F$ ) and the axial deformation ( $\Delta l$ ) of each sample were recorded until failure, utilizing a load cell with a maximum load capacity of 10 kN and a clip-on extensometer, respectively. The above-mentioned testing methodology complies with the corresponding standard EN 10002-1:2001 [32].

Subsequently, the stress ( $\sigma$ )–strain ( $\epsilon$ ) curves of the tested specimens were calculated using the obtained laboratory measurements and the following relations:

$$\sigma = \frac{F}{A_{gross}}, A_{gross} = b \times t \quad (2)$$

$$\epsilon = \frac{\Delta l}{l_0} \quad (3)$$

where  $F$  is the applied load,  $b$ ,  $t$  are the width and thickness of the specimens,  $\Delta l$  is the axial deformation, and  $l_0$  the specimen's initial length (distance between the grips).

## 3. Results and Discussion

### 3.1. Confocal Microscopy Measurements

According to the methodology outlined in Section 2.2., the confocal measurements conducted on the surface of the printed specimens revealed varying values of  $S_a$  for each specimen and across different locations. The  $S_a$  values are shown in Tables 2–4 for the different 3D-printed metals. Representative confocal measurements are shown in Figures 5–7.

**Table 2.** Sa measurements of CoCrMo specimens at different locations and magnifications.

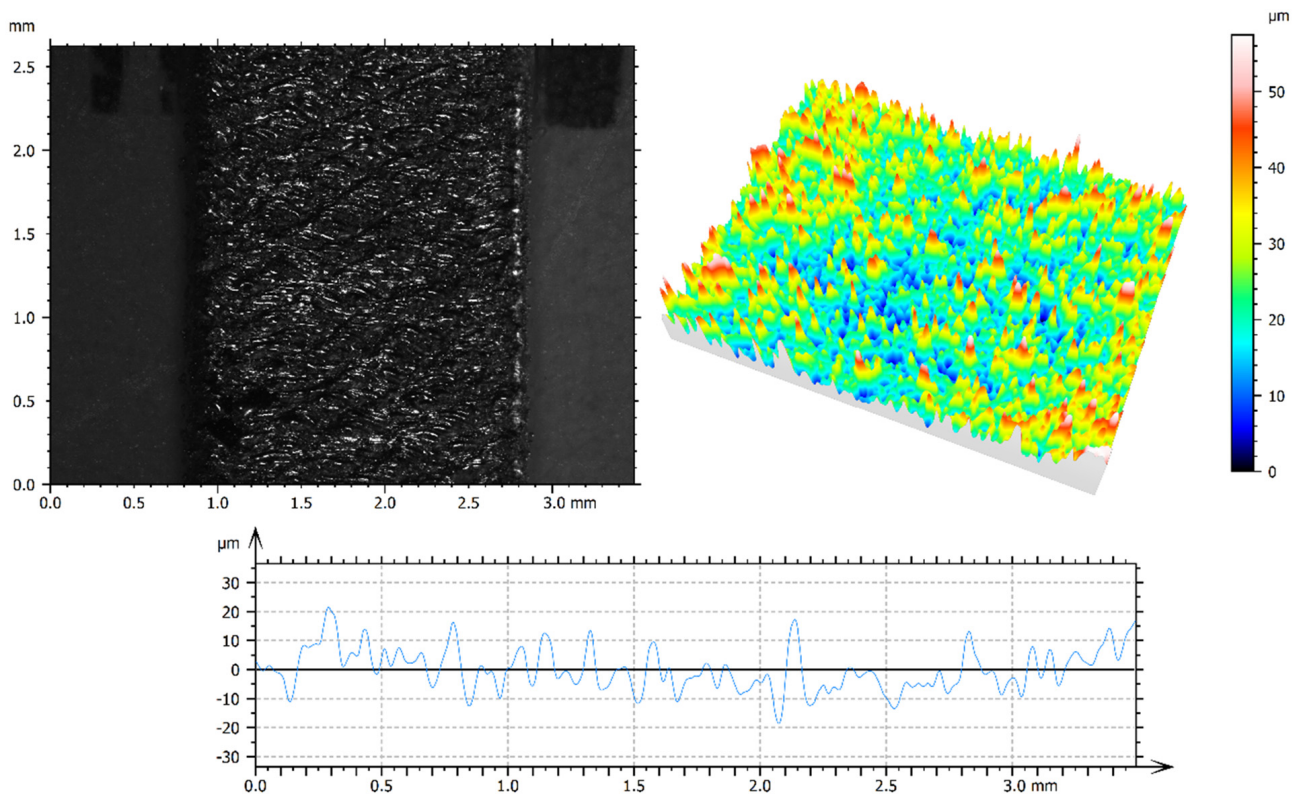
CoCrMo		Sa ( $\mu\text{m}$ )		
Magnification $\times 5$	Location #1	Location #2	Location #3	
Specimen 1	8.395	6.698	5.597	
Specimen 2	7.208	7.170	5.765	
Specimen 3	6.410	6.855	5.313	
Specimen 4	7.838	7.468	6.133	
Mean	7.463	7.048	5.702	
Magnification $\times 10$	Location #1	Location #2	Location #3	
Specimen 1	6.069	7.556	5.835	
Specimen 2	6.182	6.062	5.720	
Specimen 3	5.423	5.428	5.578	
Specimen 4	6.065	6.505	6.422	
Mean	6.065	6.388	5.888	
Magnification $\times 20$	Location #1	Location #2	Location #3	
Specimen 1	6.211	7.538	5.584	
Specimen 2	5.738	5.682	4.881	
Specimen 3	5.342	6.181	5.202	
Specimen 4	7.013	5.913	6.695	
Mean	6.076	6.328	5.591	

**Table 3.** Sa measurements of SS316L-A specimens at different locations and magnifications.

SS316L-A		Sa ( $\mu\text{m}$ )		
Magnification $\times 5$	Location #1	Location #2	Location #3	
Specimen 1	7.281	7.385	6.063	
Specimen 2	7.207	7.489	6.080	
Specimen 3	6.545	6.788	5.546	
Specimen 4	7.342	7.846	5.754	
Mean	7.094	7.385	5.861	
Magnification $\times 10$	Location #1	Location #2	Location #3	
Specimen 1	6.632	7.045	7.226	
Specimen 2	6.172	6.210	6.840	
Specimen 3	7.156	7.089	7.482	
Specimen 4	7.238	8.887	7.698	
Mean	6.800	7.308	7.312	
Magnification $\times 20$	Location #1	Location #2	Location #3	
Specimen 1	6.414	7.058	7.270	
Specimen 2	7.795	7.100	7.484	
Specimen 3	7.000	6.982	6.628	
Specimen 4	7.015	9.973	6.819	
Mean	7.056	7.778	7.050	

**Table 4.** Sa measurements of SS17-4PH-A specimens at different locations and magnifications.

SS17-4PH-A		Sa ( $\mu\text{m}$ )		
Magnification $\times 5$	Location #1	Location #2	Location #3	
Specimen 1	7.318	6.940	6.234	
Specimen 2	6.482	6.517	5.668	
Specimen 3	6.443	6.549	5.162	
Specimen 4	6.500	6.680	6.040	
Mean	6.686	6.671	5.776	
Magnification $\times 10$	Location #1	Location #2	Location #3	
Specimen 1	6.788	7.144	6.830	
Specimen 2	6.154	6.551	6.772	
Specimen 3	9.197	6.610	6.331	
Specimen 4	6.657	7.224	7.337	
Mean	7.199	6.882	6.818	
Magnification $\times 20$	Location #1	Location #2	Location #3	
Specimen 1	7.036	7.769	7.227	
Specimen 2	6.233	6.922	6.596	
Specimen 3	7.112	7.801	7.580	
Specimen 4	6.864	7.337	7.304	
Mean	6.811	7.460	7.177	

**Figure 5.** Confocal measurements of CoCrMo at  $\times 5$  magnification. **Top left:** photo; **top right:** 3D map; **bottom:** line profile.

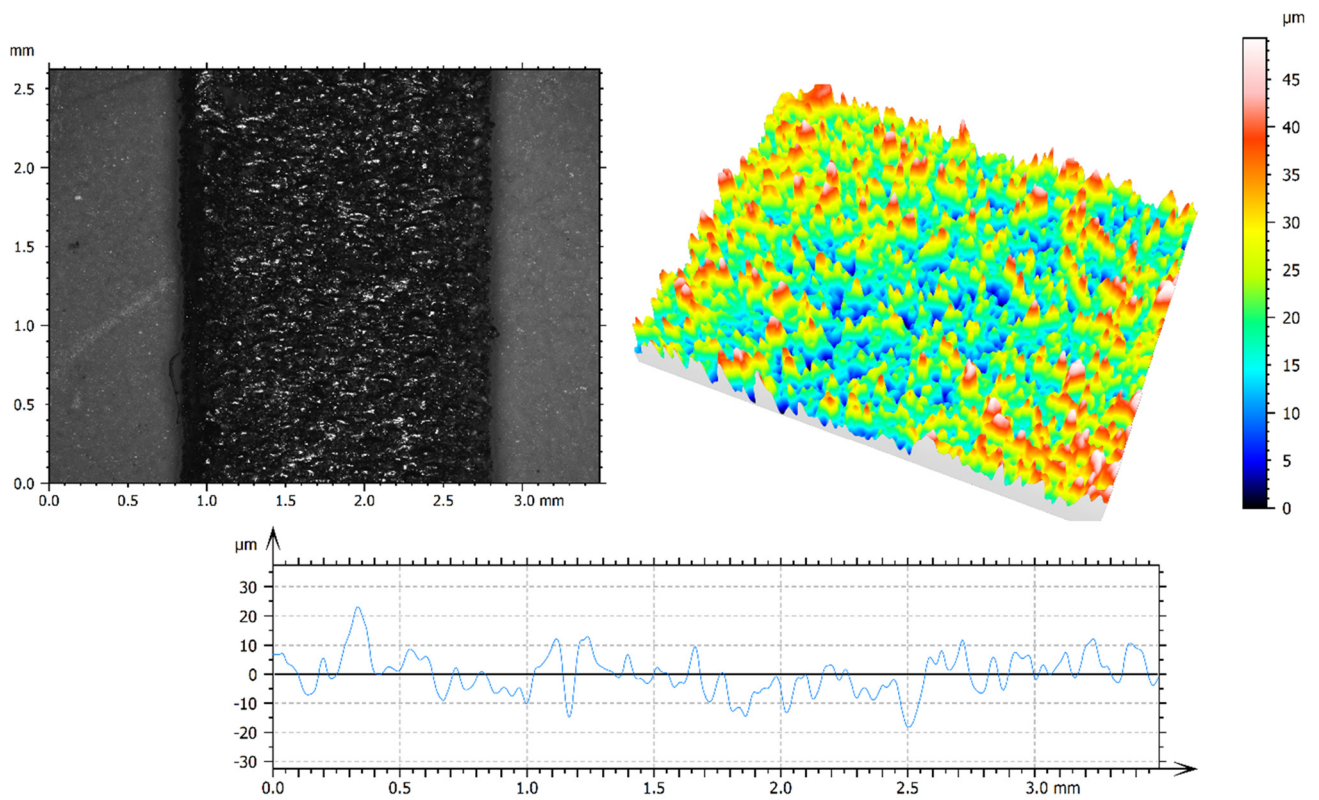


**Figure 6.** Confocal measurements of SS316L-A at  $\times 5$  magnification. **Top left:** photo; **top right:** 3D map; **bottom:** line profile.

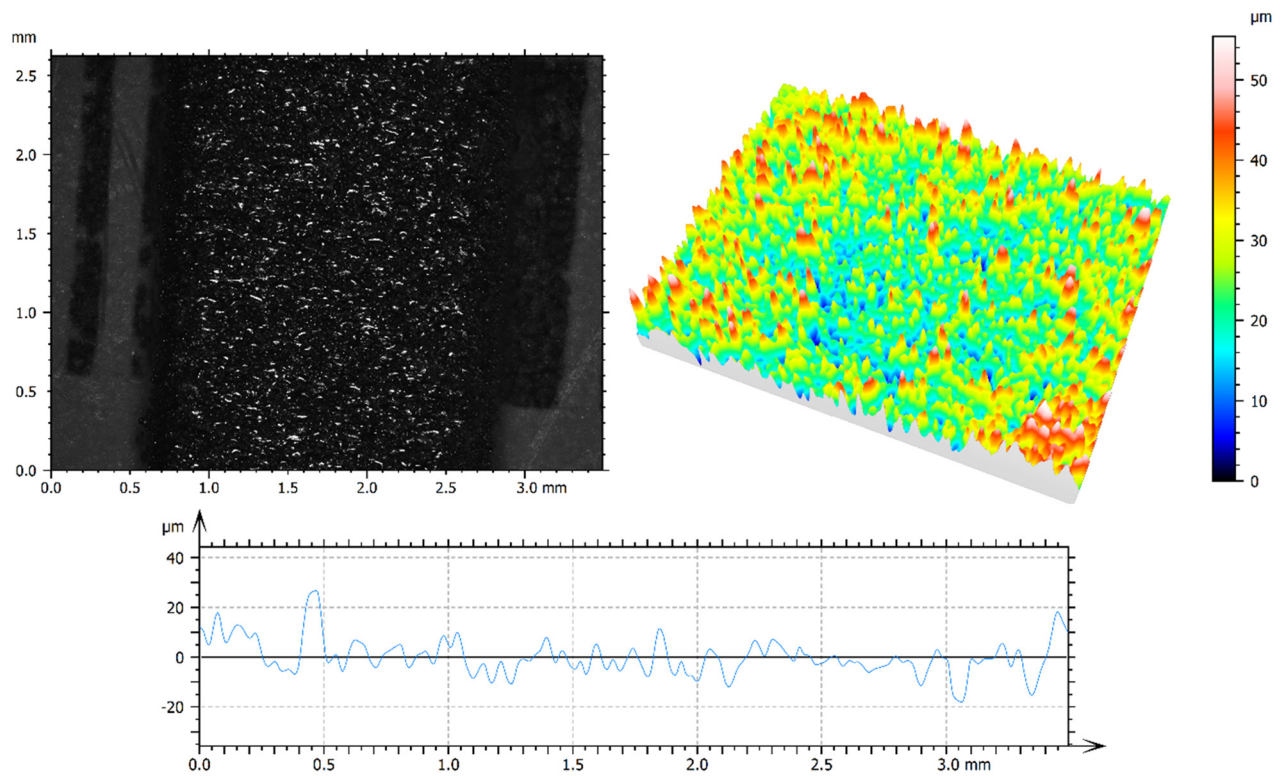


**Figure 7.** Confocal measurements of SS17-4PH-A at  $\times 5$  magnification. **Top left:** photo; **top right:** 3D map; **bottom:** line profile.

Table 2 presents all the Sa measurements obtained from three different locations of each specimen printed with CoCrMo material. Lower measurement values were observed in locations #1 and #2 for CoCrMo confocal microscopy measurements compared to location #3. This difference in values is evident not only in the mean but also in each individual specimen's measurements.

In Table 3, all the Sa measurements obtained from three different locations of each specimen printed with SS316L-A material are presented. Notably, for the specimens of this material in location #3, the smallest Sa measurement is observed only with a magnification of  $\times 5$ .

Finally, Table 4 presents the Sa measurements of the SS17-4PH-A-printed specimens. Notably, for this material, there are no significant differences in the means of the Sa measurements among different locations (#1, #2, #3).

Figures 5 and 6 present illustrations of the Sa confocal measurements of CoCrMo and SS316L-A at  $\times 5$  magnification. Both figures provide valuable insights to enhance the understanding of the uniformity in Sa values. To further enhance Sa uniformity, different VED values can be explored, as they affect the presence of molten and unmolten powder particles on the specimen's surface and the quality of the melting process [33].

In SS17-4PH-A specimens, when observing the 3D map in Figure 7, the greatest uniformity in Sa values is observed compared to the other two materials. This is also confirmed by the smaller fluctuations presented in the line profile.

Table 2 reveals that the value of Sa exhibited variations across different magnifications. In this work, the roughness at the lowest magnification ( $\times 5$ ) was used, since it was considered to be more appropriate for the (macroscopic) applications for which the specimens were 3D-printed. The mean value of Sa (from the measurements at  $\times 5$  magnification of each specimen) vs. the VED with which the specimens were produced is given in Table 5.

**Table 5.** Values of the mean Sa at  $\times 5$  magnification as well as the VED for the three metals.

CoCrMo		SS316L-A		SS17-4PH-A	
Mean Sa ( $\mu\text{m}$ )	VED ( $\text{J}/\text{mm}^3$ )	Mean Sa ( $\mu\text{m}$ )	VED ( $\text{J}/\text{mm}^3$ )	Mean Sa ( $\mu\text{m}$ )	VED ( $\text{J}/\text{mm}^3$ )
6.714	166.667	6.925	125.000	6.222	91.667
6.193	141.176	6.293	107.692	6.052	80.000
7.146	190.476	6.990	140.000	6.407	100.000

### 3.2. Quantification of the VED Effect on Surface Characteristics

In a recent study [19], the effect of the VED on the surface characteristics of Inconel specimens was assessed, and a linear behavior of the form  $Sa_{mean} = 0.043 \cdot VED + 9$  was reported. The validity of this linear behavior is tested herein for the cases of the CoCr-, SS316L-, and SS17-4PH-3D-printed metals. The mean Sa values were plotted against the respective VED and a linear fitting was applied, as shown in Figure 8.

From Figure 8, it can be seen that for CoCr, SS316L, and SS17-4PH, as well as for Inconel [19], a linear relation can be formulated between the mean Sa value and its VED, of the form

$$Sa_{mean} = a \cdot VED + b \quad (4)$$

where the various parameter values are given in Table 6.

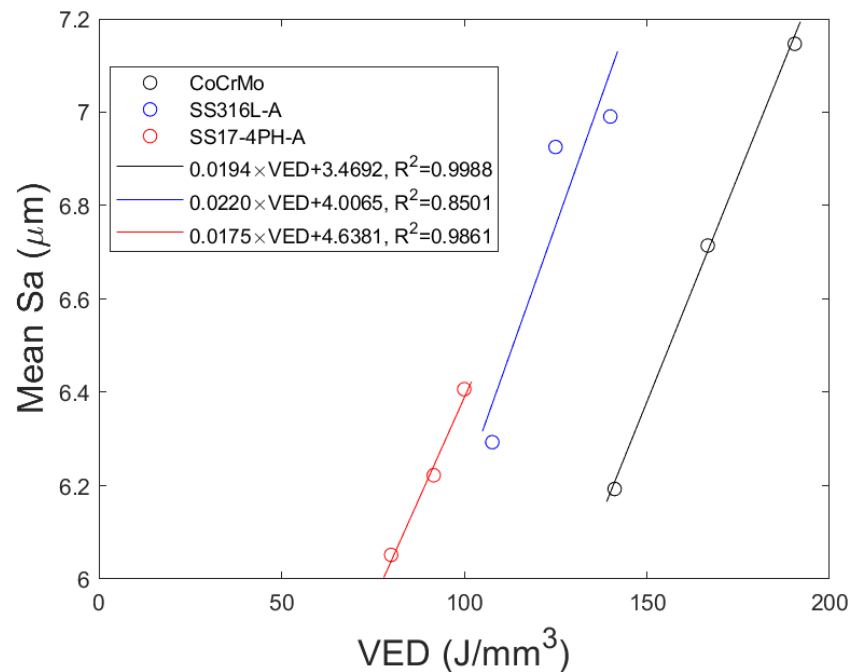


**Figure 8.** Plot of the mean Sa vs. VED for the three 3D-printed specimens.

**Table 6.** Parameters of the mean Sa vs. the VED relation for the 3D-printed specimens.

Material	a	b
CrCoMo	0.0194	3.4692
SS316L-A	0.0220	4.0065
SS17-4PH-A	0.0175	4.6381
Inconel [11]	0.0430	9.0000

### 3.3. Tensile Deformation Measurements

In order to conduct the experiment according to the methodology described in Section 2.3, obtaining the dimensions of all tested specimens is crucial. This requirement is essential to efficiently use the testing machine and comply with the relevant standard for tensile measurements. All tested specimens' dimensions were measured using a digital caliper, and their geometrical characteristics are given in Table 7.

**Table 7.** List of all examined specimens and their measured dimensions.

Material	Batch	Specimen	Width b (mm)	Thickness t (mm)	Grips Distance $l_0$ (mm)
CoCrMo	S1	1	2.07	1.05	23
		2	2.05	1.02	23
		3	2.05	1.06	21
	S2	1	2.03	1.02	21
		2	2.00	1.00	19
		3	2.04	1.03	28
	S3	1	2.07	1.07	19
		2	1.92	0.93	20
		3	1.95	0.94	19

Table 7. Cont.

Material	Batch	Specimen	Width b (mm)	Thickness t (mm)	Grips Distance $l_0$ (mm)
SS316L-A	S1	1	1.92	0.90	20
		2	2.05	1.02	23
		3	1.93	0.93	19
	S2	1	1.94	0.93	20
		2	1.95	0.91	20
		3	1.89	0.93	20
	S3	1	1.93	0.90	21
		2	1.92	0.93	20
		3	1.95	0.94	19
SS17-4PH-A	S1	1	2.20	1.17	23
		2	2.13	1.15	20
		3	2.20	1.19	20
	S2	1	2.17	1.15	22
		2	2.17	1.16	21
		3	2.20	1.15	20
	S3	1	2.21	1.18	24
		2	2.16	1.17	20
		3	2.17	1.16	19

Typical stress–strain curves for the three types of 3D-printed metals at hand, as depicted in Figures 9–11. The obtained curves are used to calculate the modulus of elasticity ( $E$ ), the yield stress ( $\sigma_y$ ), the strain at yield ( $\epsilon_y$ ), the tensile strength ( $\sigma_u$ ), and the strain at maximum stress ( $\epsilon_u$ ). These properties are given in Table 8 for each tested specimen.

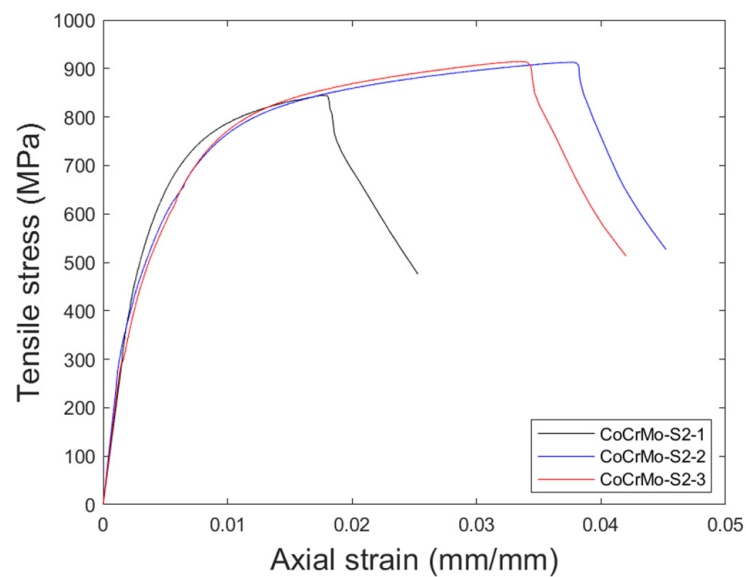


Figure 9. Stress–strain response of the experimentally tested 3D-printed CoCrMo specimens.

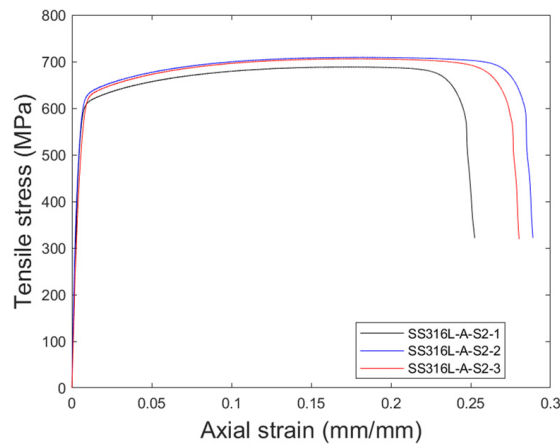


Figure 10. Stress–strain response of the experimentally tested 3D-printed SS316L-A specimens.

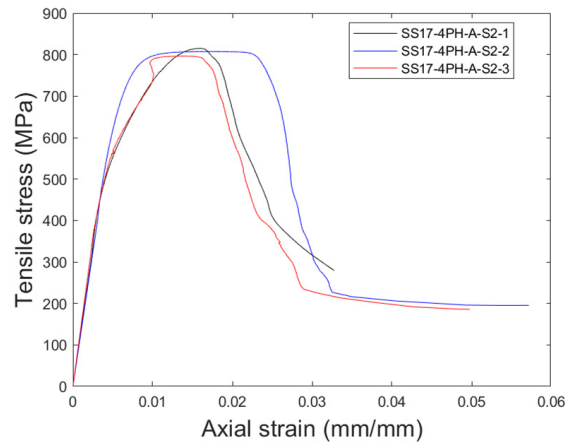


Figure 11. Stress–strain response of the experimentally tested 3D-printed SS17-4PH-A specimens.

Table 8. Mechanical properties of the 3D-printed metals.

Material	Batch	Specimen	$E$ (MPa)	$\sigma_y$ (MPa)	$\epsilon_y$ (mm/mm)	$\sigma_u$ (MPa)	$\epsilon_u$ (mm/mm)
CoCrMo	S1	1	123,571	703.01	0.0057	899.48	0.0232
		2	141,030	632.37	0.0045	893.46	0.0192
		3	92,071	693.30	0.0075	906.44	0.0325
		average	118,891	676.23	0.0059	899.79	0.025
		deviation	±17%	±5%	±21%	±1%	±22%
	S2	1	119,252	679.68	0.0057	845.31	0.0177
		2	230,902	666.35	0.0066	913.40	0.0374
		3	207,308	649.90	0.0063	915.14	0.0335
		average	185,820	665.31	0.0062	891.29	0.030
		deviation	±26%	±2%	±6%	±4%	±29%
	S3	1	133,283	653.44	0.0049	928.32	0.0369
		2	201,262	857.37	0.0043	1061.11	0.0386
		3	116,622	869.14	0.0075	1124.65	0.0412
		average	150,389	793.32	0.0055	1038.03	0.039
		deviation	±24%	±12%	±25%	±8%	±5%

Table 8. Cont.

Material	Batch	Specimen	$E$ (MPa)	$\sigma_y$ (MPa)	$\epsilon_y$ (mm/mm)	$\sigma_u$ (MPa)	$\epsilon_u$ (mm/mm)
SS316L-A	S1	1	118,713	658.86	0.0056	778.63	0.1898
		2	85,153	513.69	0.0060	605.17	0.1573
		3	61,997	611.78	0.0099	728.80	0.1867
		average	88,621	594.78	0.0072	704.20	0.178
		deviation	±26%	±10%	±27%	±10%	±8%
	S2	1	85,635	587.46	0.0069	689.30	0.1753
		2	70,456	622.83	0.0088	710.11	0.1824
		3	66,349	611.74	0.0092	706.88	0.1783
		average	74,147	607.34	0.0083	702.09	0.179
		deviation	±11%	±2%	±12%	±1%	±2%
	S3	1	110,083	661.91	0.0060	757.13	0.1196
		2	87,681	648.84	0.0074	741.08	0.2013
		3	93,181	679.38	0.0073	781.58	0.2231
		average	96,982	663.38	0.0069	759.93	0.181
		deviation	±10%	±2%	±9%	±2%	±25%
SS17-4PH-A	S1	1	113,286	740.40	0.0065	859.06	0.0304
		2	83,734	839.85	0.0100	912.45	0.0400
		3	112,212	777.63	0.0069	843.53	0.0191
		average	103,077	785.96	0.0078	871.68	0.030
		deviation	±13%	±5%	±20%	±3%	±29%
	S2	1	113,168	542.38	0.0048	815.84	0.0160
		2	107,638	727.12	0.0068	808.25	0.0178
		3	110,626	563.08	0.0051	797.15	0.0132
		average	110,477	610.86	0.0055	807.08	0.016
		deviation	±2%	±14%	±16%	±1%	±12%
	S3	1	80,180	519.57	0.0065	890.91	0.0434
		2	110,732	471.72	0.0043	890.03	0.0564
		3	83,278	829.58	0.0100	910.37	0.0513
		average	91,397	606.95	0.0069	897.10	0.050
		deviation	±15%	±26%	±34%	±1%	±11%

### 3.4. Quantification of the VED Effect on Mechanical Characteristics

Upon conducting the mechanical tests as outlined in the methodology outlined in Section 2.3, conclusions can be drawn regarding how the tensile measurements of the specimens are related to the VED. In the context of mechanical properties, yield stress is the limit of the elastic region and toughness (hardness) is the energy per unit volume transferred to the material through mechanical loading and calculated as the area under the stress–strain curve. It is worth noting that roughness is a surface attribute, whereas toughness is a mechanical property.

Considering the connection that should exist between the VED and the mechanical characteristics of the 3D-printed metals at hand, a relation was sought between the VED and yield stress, as well as between the VED and toughness (calculated as the integral

under the stress–strain curve until the point of maximum stress). The plots of (a) yield stress vs. VED, and (b) toughness vs. VED, for each metal are given in Figures 12 and 13.

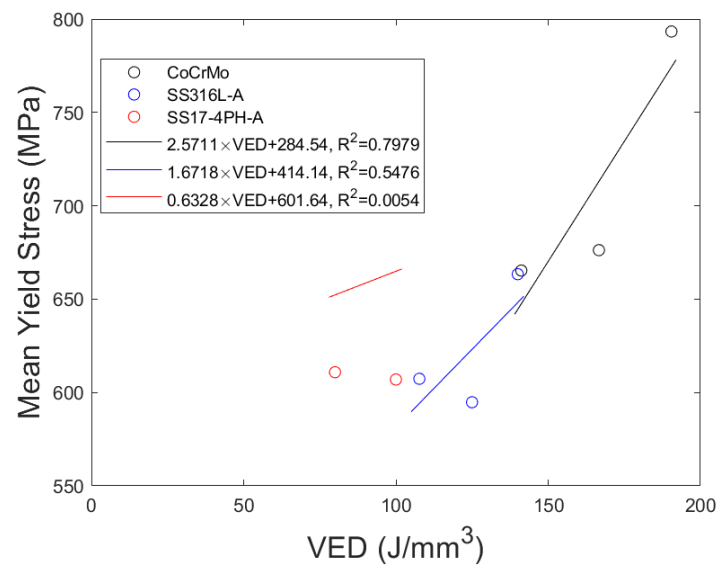


**Figure 12.** Plot of the mean yield stress vs. VED for the three 3D-printed specimens.

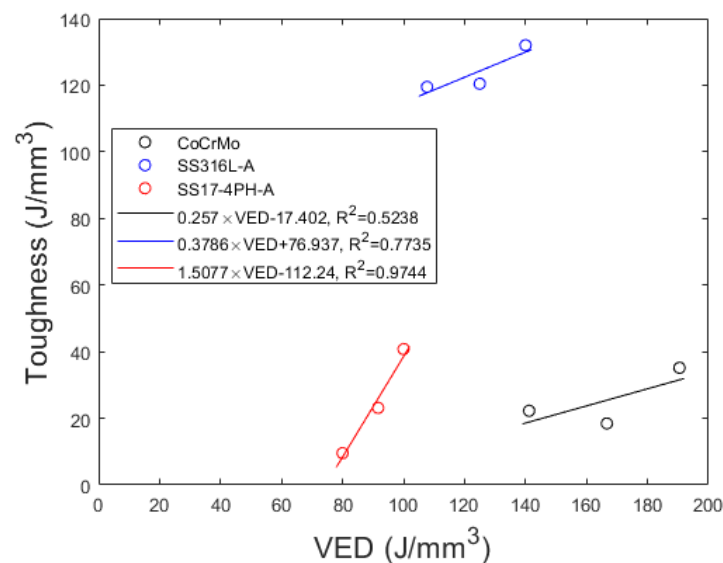


**Figure 13.** Plot of the mean toughness vs. VED for the three 3D-printed specimens.

As a first approximation, a linear relation between the mean yield stress as well as the mean toughness with the VED was sought. From Figures 12 and 13, linear relations of the form

$$\sigma_y = c \cdot VED + d \quad (5)$$

$$Toughness = e \cdot VED + f \quad (6)$$

can be formulated, with the various parameter values given in Table 9.

By appropriately controlling the VED during the printing process, Equations (5) and (6) can provide an approximate value for the yield stress and toughness, as well as the surface quality, of the printed specimens. This will aid manufacturers in producing specimens of better quality, minimizing the effort and loss of material.

**Table 9.** Parameters of the linear relations between the yield stress and the VED and the toughness and the VED for the three printed specimens.

Material	c	d	e	f
CoCrMo	2.5711	284.54	0.257	−17.402
SS316L-A	1.6718	414.14	0.3786	76.967
SS17-4PH-A	0.6328	601.64	1.5077	−112.24

#### 4. Conclusions

The present study investigates the correlation between the VED, surface roughness, and mechanical properties in 3D-printed stainless steel 316L-A, stainless steel 17-4PH-A, and CoCrMo alloy, fabricated via SLM. Different VED values were achieved by adjusting the 3D printing parameters of laser power and laser speed, allowing conclusions to be drawn about their effect on their mechanical performance. A linear relation between VED and surface roughness, first proposed in [19] for Inconel-printed specimens, was verified herein for the case of SS316L-A, SS17-4PH-A, and CoCrMo alloy specimens. The first conclusion is that, by increasing the VED, surface roughness also increases linearly, thus leading to printed specimens with reduced surface quality. While this work offers valuable insights into the optimization of the SLM process based on the VED values, it is crucial to consider that surface roughness, yield stress, and toughness also exhibit linear changes. As a first approximation, a linear relation was also deduced and proposed herein, between the VED and the specimens' yield stress and toughness. This indicates that, by increasing the VED value, at least within the 80–190 J/mm<sup>3</sup> range, the specimens' yield stress as well as their toughness increases. Of course, more VED values need to be employed in order for the exact relation (linear or non-linear) between the VED and yield stress/toughness to be established. The experiments demonstrate that increasing the VED value negatively affects surface quality, but improves mechanical performance (yield stress and toughness). This observation is supported by the examination of how the VED influences mechanical performance and surface roughness across the three different materials. Nevertheless, further experiments are needed to calculate the exact non-linear relation between the VED and toughness or yield stress in these as well as in other metallic materials utilized by the SLM technique, taking into account their structural and morphological characteristics. The exact relationship would necessitate the use of VED values much different from those examined in the present work, which are around the VED value suggested by the 3D printer's manufacturer for each material. This issue will be addressed in future research.

This work provides a means for predicting the quality of 3D-printed metal and alloy specimens in terms of their surface roughness and mechanical properties, which can be utilized by fabricators to make an optimized selection between the needed surface quality and the expected mechanical strength. By leveraging this approach, the need for 3D-printing physical samples to assess mechanical parameters is eliminated, along with the reduction in costs and time associated with the 3D printing process. This is especially pronounced in applications where surface quality and strength are of crucial significance.

**Author Contributions:** Conceptualization, A.A.K. and E.M.P.; methodology, A.A.K. and E.M.P.; software, A.A.K. and S.P.; validation, K.K.; formal analysis, L.M.; investigation, S.P. and L.M.; resources, E.M.P.; data curation, A.A.K. and L.M.; writing—original draft preparation, E.M.P. and S.P.; writing—review and editing, A.A.K. and L.M.; visualization, A.A.K. and S.P.; supervision, D.T.; project administration, E.M.P.; funding acquisition, E.M.P. All authors have read and agreed to the published version of the manuscript.

**Funding:** European Regional Development Fund (ERDF) of the European Union for the implementation of its project under the Action “Investment Plans of Innovation” in the Region of Central Macedonia, under the framework of the Operational Program “Central Macedonia 2014–2020”: no.KMP6-0232019.

**Data Availability Statement:** Data available on request.

**Conflicts of Interest:** The authors declare no conflict of interest.

## References

1. ISO/ASTM52900-15; Standard Terminology for Additive Manufacturing—General Principles—Terminology. ASTM International: West Conshohocken, PA, USA, 2015.
2. Huber, M.; Ess, J.; Hartmann, M.; Würms, A.; Rettberg, R.; Kränzler, T.; Löffel, K. Process setup for manufacturing of a pump impeller by selective laser melting. In *Industrializing Additive Manufacturing—Proceedings of Additive Manufacturing in Products and Applications—AMPA2017*; Springer: Cham, Switzerland, 2018; pp. 252–263. [\[CrossRef\]](#)
3. Khanoki, S.A.; Pasini, D. Fatigue design of a mechanically biocompatible lattice for a proof-of-concept femoral stem. *J. Mech. Behav. Biomed. Mater.* **2013**, *22*, 65–83. [\[CrossRef\]](#)
4. Fotovvati, B.; Balasubramanian, M.; Asadi, E. Modeling and Optimization Approaches of Laser-Based Powder-Bed Fusion Process for Ti-6Al-4V Alloy. *Coatings* **2020**, *10*, 1104. [\[CrossRef\]](#)
5. Yao, D.; Liu, X.; Wang, J.; Fan, W.; Li, M.; Fu, H.; Zhang, H.; Yang, X.; Zou, Q.; An, X. Numerical insights on the spreading of practical 316 L stainless steel powder in SLM additive manufacturing. *Powder Technol.* **2021**, *390*, 197–208. [\[CrossRef\]](#)
6. Ahmadi, M.; Tabary, S.A.A.B.; Rahmatabadi, D.; Ebrahimi, M.S.; Abrinia, K.; Hashemi, R. Review of selective laser melting of magnesium alloys: Advantages, microstructure and mechanical characterizations, defects, challenges, and applications. *J. Mater. Res. Technol.* **2022**, *19*, 1537–1562. [\[CrossRef\]](#)
7. Gokuldoss, P.K.; Kolla, S.; Eckert, J. Additive Manufacturing Processes: Selective Laser Melting, Electron Beam Melting and Binder Jetting—Selection Guidelines. *Materials* **2017**, *10*, 672. [\[CrossRef\]](#)
8. Leo, P.; Cabibbo, M.; Del Prete, A.; Giganto, S.; Martínez-Pellitero, S.; Barreiro, J. Laser Defocusing Effect on the Microstructure and Defects of 17-4PH Parts Additively Manufactured by SLM at a Low Energy Input. *Metals* **2021**, *11*, 588. [\[CrossRef\]](#)
9. Kladovasilakis, N.; Charalampous, P.; Kostavelis, I.; Tzetzis, D.; Tzovaras, D. Impact of metal additive manufacturing parameters on the powder bed fusion and direct energy deposition processes: A comprehensive review. *Prog. Addit. Manuf.* **2021**, *6*, 349–365. [\[CrossRef\]](#)
10. Ninpetch, P.; Kowitwarangkul, P.; Mahathanabodee, S.; Chalermkarannon, P.; Ratanadecho, P. A review of computer simulations of metal 3D printing. In Proceedings of the Second Materials Research Society of Thailand International Conference, Pattaya, Thailand, 10–12 July 2019; p. 050002. [\[CrossRef\]](#)
11. Singh, R.; Gupta, A.; Tripathi, O.; Srivastava, S.; Singh, B.; Awasthi, A.; Rajput, S.K.; Sonia, P.; Singhal, P.; Saxena, K.K. Powder bed fusion process in additive manufacturing: An overview. *Mater. Today Proc.* **2020**, *26*, 3058–3070. [\[CrossRef\]](#)
12. Yerubayeva, A.; Shehab, E.; Ali, H. Recent advances and application of Selective Laser Melting (SLM) technology in the aerospace industry. In Proceedings of the International Conference on Informatics, Technology, and Engineering 2021 (InCITE 2021), Surabaya, Indonesia, 25–26 August 2021; p. 030002. [\[CrossRef\]](#)
13. Tian, Q. The Development Status of Selective Laser Melting Technology (SLM). *J. Phys. Conf. Ser.* **2021**, *1798*, 012045. [\[CrossRef\]](#)
14. Ma, Z.; Gao, M.; Guo, K.; Wang, Q.; Li, L.; Liu, C.; Zhu, G.; Liu, Z. Analysis and Optimization of Energy Consumption for Multi-part Printing Using Selective Laser Melting and Considering the Support Structure. *Int. J. Precis. Eng. Manuf. Green Technol.* **2023**, *10*, 693–707. [\[CrossRef\]](#)
15. Mamo, H.B.; Adamiak, M.; Kunwar, A. 3D printed biomedical devices and their applications: A review on state-of-the-art technologies, existing challenges, and future perspectives. *J. Mech. Behav. Biomed. Mater.* **2023**, *143*, 105930. [\[CrossRef\]](#)
16. Rajendran, S.; Palani, G.; Kanakaraj, A.; Shanmugam, V.; Veerasimman, A.; Gadek, S.; Korniejenko, K.; Marimuthu, U. Metal and Polymer Based Composites Manufactured Using Additive Manufacturing—A Brief Review. *Polymers* **2023**, *15*, 2564. [\[CrossRef\]](#)
17. La Fé-Perdomo, I.; Ramos-Grez, J.A.; Beruvides, G.; Mujica, R.A. Selective laser melting: Lessons from medical devices industry and other applications. *Rapid Prototyp. J.* **2021**, *27*, 1801–1830. [\[CrossRef\]](#)
18. Gao, B.; Zhao, H.; Peng, L.; Sun, Z. A Review of Research Progress in Selective Laser Melting (SLM). *Micromachines* **2022**, *14*, 57. [\[CrossRef\]](#) [\[PubMed\]](#)
19. Pechlivani, E.M.; Kampouris, A.K.; Melidis, L.; Katakalos, K.; Kontodina, T.; Tzovaras, D.; Konstantinidis, A.A. 3D printed Inconel mechanical response related to volumetric energy density. *Mater. Today Proc.* **2023**. [\[CrossRef\]](#)
20. Nasiri, S.; Khosravani, M.R. Machine learning in predicting mechanical behavior of additively manufactured parts. *J. Mater. Res. Technol.* **2021**, *14*, 1137–1153. [\[CrossRef\]](#)
21. Fielden-Stewart, Z.; Coope, T.; Bacheva, D.; Kim, B.C. Effect of the surface morphology of SLM printed aluminium on the interfacial fracture toughness of metal-composite hybrid joints. *Int. J. Adhes. Adhes.* **2021**, *105*, 102779. [\[CrossRef\]](#)
22. Zhang, S.; Zhang, S.; Li, F.; Li, Z.; Wang, Y.; Liu, B. Selective Laser Melting of Al-Cu-Mn-Mg Alloys: Processing and Mechanical Properties. *Metals* **2023**, *13*, 1520. [\[CrossRef\]](#)
23. Ozsoy, A.; Yasa, E.; Keles, M.; Tureyen, E.B. Pulsed-mode Selective Laser Melting of 17-4 PH stainless steel: Effect of laser parameters on density and mechanical properties. *J. Manuf. Process.* **2021**, *68*, 910–922. [\[CrossRef\]](#)
24. Ghayoor, M.; Lee, K.; He, Y.; Chang, C.; Paul, B.K.; Pasebani, S. Selective laser melting of 304L stainless steel: Role of volumetric energy density on the microstructure, texture and mechanical properties. *Addit. Manuf.* **2020**, *32*, 101011. [\[CrossRef\]](#)

25. Didier, P.; Le Coz, G.; Robin, G.; Lohmuller, P.; Piotrowski, B.; Moufki, A.; Laheurte, P. Consideration of SLM additive manufacturing supports on the stability of flexible structures in finish milling. *J. Manuf. Process.* **2021**, *62*, 213–220. [[CrossRef](#)]
26. Gong, H.; Rafi, K.; Gu, H.; Starr, T.; Stucker, B. Analysis of defect generation in Ti–6Al–4V parts made using powder bed fusion additive manufacturing processes. *Addit. Manuf.* **2014**, *1–4*, 87–98. [[CrossRef](#)]
27. Order MetcoAdd 75A Additive Manufacturing Powder Online at myMetco. (n.d.). Available online: <https://mymetco-europe.oerlikon.com/en-us/product/metcoadd75a?isRegionSelection> (accessed on 27 July 2023).
28. Order MetcoAdd 316L-A Additive Manufacturing Powder Online at myMetco. (n.d.). Available online: <https://mymetco-europe.oerlikon.com/en-us/product/metcoadd316la?isRegionSelection> (accessed on 27 July 2023).
29. Order METCOADD 17-4PH-A Additive Manufacturing Powder Online at myMetco. (n.d.). Available online: <https://mymetco-europe.oerlikon.com/en-us/product/metcoadd174pha> (accessed on 27 July 2023).
30. Chen, F.; Wang, Q.; Zhang, C.; Huang, Z.; Jia, M.; Shen, Q. Microstructures and mechanical behaviors of additive manufactured Inconel 625 alloys via selective laser melting and laser engineered net shaping. *J. Alloys Compd.* **2022**, *917*, 165572. [[CrossRef](#)]
31. Papadimitriou, C.; Melidis, L.; Kotoulas, L.; Makris, N.; Katakalos, K. Thermomechanical Characterization of CFRPs under Elevated Temperatures for Strengthening Existing Structures. *Fibers* **2021**, *9*, 80. [[CrossRef](#)]
32. *EN 10002-1:2001*; Metallic Materials—Tensile Testing—Part 1: Method of Test (at Ambient Temperature). CEN—European Committee for Standardization: Brussels, Belgium, 2001.
33. Sun, D.; Gu, D.; Lin, K.; Ma, J.; Chen, W.; Huang, J.; Sun, X.; Chu, M. Selective laser melting of titanium parts: Influence of laser process parameters on macro- and microstructures and tensile property. *Powder Technol.* **2019**, *342*, 371–379. [[CrossRef](#)]

**Disclaimer/Publisher’s Note:** The statements, opinions and data contained in all publications are solely those of the individual author(s) and contributor(s) and not of MDPI and/or the editor(s). MDPI and/or the editor(s) disclaim responsibility for any injury to people or property resulting from any ideas, methods, instructions or products referred to in the content.